

Coexistence of large negative and positive magnetodielectric response in $\text{Bi}_{1-x}\text{Ca}_x\text{Fe}_{1-y}\text{Ti}_y\text{O}_{3-\delta}$ nanoparticle ceramics

Subhajit Nandy,^{1,*} Pavana S. V. Mocherla,^{1,*} E. Abdelhamid,² B. Nadgorny,² R. Naik² and C. Sudakar^{1,†}

¹Multifunctional Materials Laboratory, Department of Physics, Indian Institute of Technology Madras, Chennai 600036, India

²Department of Physics and Astronomy, Wayne State University, Detroit, Michigan 48202, USA



(Received 8 January 2021; revised 19 March 2021; accepted 19 April 2021; published 6 May 2021)

Magnetodielectric (MD) properties of as-prepared (AP) and air-annealed $\text{Bi}_{1-x}\text{Ca}_x\text{Fe}_{1-y}\text{Ti}_y\text{O}_{3-\delta}$ nanoparticle ceramics made by spark plasma sintering process are investigated as a function of temperature. Aliovalent Ca^{2+} substitution at Bi^{3+} site creates oxygen vacancies (V_O) in the lattice disrupting the intrinsic spin cycloid of BiFeO_3 , which are suppressed when the charge compensating Ti^{4+} is co-substituted. In addition, cation substitution reduces the grain size and increases surface oxygen vacancies. These lattice and surface V_O defects play a significant role in enhancing the magnetic properties. Zero-field-cooled magnetization curves of all AP samples show a sharp Verwey-like transition at ~ 120 K, which weakens on air-annealing. A coexistence of positive and negative MD [$\text{MD} = \frac{\Delta\varepsilon(H)}{\varepsilon(H=0)}$; $\Delta\varepsilon(H) = \varepsilon(H) - \varepsilon(H=0)$] response is observed, with the former dominating at 300 K and the latter at 10 K. As-prepared 5 at.% (10 at.%) Ca and Ca-Ti substituted BiFeO_3 ceramics exhibit a maximum MD response of -10% ($\sim +3\%$) at 10 K (300 K). Negative MD response diminishes for air-annealed $\text{Bi}_{1-x}\text{Ca}_x\text{Fe}_{1-y}\text{Ti}_y\text{O}_{3-\delta}$ ceramics due to the reduction in V_O concentration. Samples exhibiting dominant positive MD response show a similar trend for MD vs H and M^2 vs H plots. This agreement between M^2 and $\Delta\varepsilon(H)$ demonstrates a strong inherent MD coupling. On the contrary, negative MD does not follow this trend yet shows a linear relationship of MD vs M^2 , suggesting a strong coupling between the magnetic and dielectric properties. Temperature-dependent MD studies carried out at 5 T show a gradual change from negative to positive values. Negative MD at low temperatures could be activated by the spin-lattice coupling, which dominates even at high frequency (1 MHz) under the applied field. Other contributions, including Verwey-like transition, magnetoresistance, and Maxwell-Wagner effects, do not influence the observed MD response. A prominent role of oxygen vacancies in altering the MD behavior of BiFeO_3 is discussed in detail.

DOI: [10.1103/PhysRevB.103.184406](https://doi.org/10.1103/PhysRevB.103.184406)

I. INTRODUCTION

Several ferroic order parameters (like ferromagnetism, ferroelectricity, ferroelasticity) are coupled strongly in multiferroic materials. Materials that exhibit strong coupling between ferroelectric and ferromagnetic properties are called magnetoelectric (ME) materials [1,2]. They have attracted enormous interest due to their wide range of applications in various fields, including spintronic devices, memory storage, actuators, and sensors [3–9]. The magnetic field effect on ferroelectric polarization or electric field on the magnetic property is gauged via the ME effect. Often, the dielectric constant (ε) of a given material is investigated as a function of temperature in the presence and absence of a magnetic field to understand the ME effect [10–12]. ME materials are broadly categorized into two types: (i) composite materials [13–16] and (ii) single-phase multiferroics [17–19]. BiFeO_3 captured attention as a single-phase multiferroic system due to the coexistence of antiferromagnetism with high $T_N \sim 643$ K and ferroelectricity with $T_C \sim 1103$ K [20].

Several studies on magnetic, electrical, and MD properties have been carried out on single-phase BiFeO_3 [21,22].

Substituting at Bi or Fe sites, or cosubstituting both of them with appropriate metal cations is a strategy used to enhance the magnetic and MD properties [17,23–26]. Singh *et al.*'s work on as-grown Ba-doped BiFeO_3 showed better ME properties in oxygen vacancy-rich samples compared to those of oxygen annealed pellets [27]. A negative MD coefficient of 6.5%, observed in $\text{BiFe}_{0.75}\text{Ni}_{0.25}\text{O}_3$ nanoceramics, demonstrates a strong coupling between the magnetic and dielectric properties [28]. This has been attributed to the creation of oxygen vacancy with increasing Ni concentration. Dutta *et al.* [25] attributed the highest MD coupling of 6% measured at 2.5 T in $\text{Sm}(5\%):\text{Zr}(5\%)$ codoped BiFeO_3 to the structural strain arising from the lattice parameter variation due to doping. Mukherjee *et al.* [29] also showed a maximum of 5.8% MD coefficient at 1.5 T for Y-Mn co-doped BiFeO_3 .

Various parameters are considered to be the contributing sources of the observed MD property in multifunctional materials. Of these, magnetoelectric coupling, magnetoresistance and Maxwell-Wagner mechanism are primarily important [30,31]. Change in the sample dimensions in the presence of the magnetic field, known as magnetostriction, is also considered as one of the origins for the observed MD effect [31]. Catalan *et al.* have observed magnetocapacitance without any magnetoelectric coupling, where a combination of magnetoresistance and Maxwell-Wagner effect is shown to produce such a MD effect [30]. The resistive contribution to the MD

*These authors contributed equally to this work.

†csudakar@iitm.ac.in

effect has also been observed in nonmultiferroic materials [32].

In this manuscript, we discuss the magnetic, dielectric, and MD effect of as-prepared (AP) and air-annealed (AA) $\text{Bi}_{1-x}\text{Ca}_x\text{Fe}_{1-y}\text{Ti}_y\text{O}_{3-\delta}$ (BCFO: $0 \leq x \leq 0.1$, $y = 0$; and BCFTO: $0 \leq x \leq 0.1$ with $x = y$) ceramics prepared via spark plasma sintering (SPS) process. Oxygen vacancies (V_O) are created due to the aliovalent dopant (Ca^{2+}) substitution in BCFO. These sintered ceramics show enhancement in the saturation magnetization with increasing concentration of Ca^{2+} and Ca^{2+} - Ti^{4+} . The effect of increased surface V_O due to the reduction of grain sizes is also shown to play a major role in enhancing the magnetic properties in $\text{Bi}_{1-x}\text{Ca}_x\text{Fe}_{1-y}\text{Ti}_y\text{O}_{3-\delta}$ ceramics. V_O defects can be suppressed through air annealing, which also shows a reduction in the magnetization of air-annealed BCFTO ceramics. Zero-field-cooled (ZFC) magnetization measurements on $\text{Bi}_{1-x}\text{Ca}_x\text{Fe}_{1-y}\text{Ti}_y\text{O}_{3-\delta}$ ceramics show a sharp change at 120 K, similar to Verwey transition [33]. Further, we note a high negative MD effect [$\frac{\Delta\varepsilon(H)}{\varepsilon(H=0)} \cong -10\%$ at 5 T; where $\Delta\varepsilon(H) = \varepsilon(H) - \varepsilon(H=0)$] in as-prepared ceramics at low temperature (10 K). The negative MD effect switches to a positive effect with $\frac{\Delta\varepsilon(H)}{\varepsilon(H=0)} = +3.4\%$ at 5 T when measured at high temperature (300 K). Diminishing MD response noted in air-annealed ceramics is attributed to the reduction of V_O on air-annealing. The observed linear behavior in $\frac{\Delta\varepsilon(H)}{\varepsilon(H=0)}$ vs M^2 indicates a strong magnetoelectric coupling in $\text{Bi}_{1-x}\text{Ca}_x\text{Fe}_{1-y}\text{Ti}_y\text{O}_{3-\delta}$ ceramics.

II. EXPERIMENT

$\text{Bi}_{1-x}\text{Ca}_x\text{Fe}_{1-y}\text{Ti}_y\text{O}_{3-\delta}$ [(i) $x = y = 0$ (BFO), (ii) $x = 0.05$; $y = 0$ (BC5FO), (iii) $x = 0.1$; $y = 0$ (BC10FO), (iv) $x = y = 0.05$ (BC5FT5O) and (v) $x = y = 0.1$ (BC10FT100)] nanoparticles were prepared *via* a low-temperature citrate-based sol-gel method as reported by Nandy *et al.* [34–36]. These nanoparticles were pressed into dense pellets by the SPS technique. A uniaxial pressure of 40 MPa is applied for 5 min in vacuum at 650 °C to the powder loaded in a graphitic die of 20-mm diameter. A detailed description of the sintering process and conditions used are reported elsewhere [34,35]. These samples are referred to AP SPS pellets. After polishing and annealing in air at 550 °C for 15 minutes, the samples are referred to as AA SPS pellets. All these SPS ceramic samples are hereafter referred to as BCXFO and BCXFTYO; X and Y in the nomenclature implying the Ca and Ti dopant concentration, respectively. For example, BC5FO-AP and BC5FO-AA correspond to AP and AA $\text{Bi}_{1-x}\text{Ca}_x\text{Fe}_{1-y}\text{Ti}_y\text{O}_{3-\delta}$ with $x = 0.05$; $y = 0$; BC5FT100 correspond to $\text{Bi}_{1-x}\text{Ca}_x\text{Fe}_{1-y}\text{Ti}_y\text{O}_{3-\delta}$ with $x = 0.05$; $y = 0.10$ sample and so on. X-ray diffraction and Raman spectral studies confirm the presence of distorted rhombohedral phase in all the SPS pellets. Detailed structural and microstructural analyses on these samples were presented elsewhere [37]. Supplemental Material [38] Sec. I, Figs. S1 to S3 summarize these results. Our extensive analyses presented in the previous studies [34,35,37,39] (also summarized in Supplemental Material Sec. II [38]) have shown that BCFO pellets are oxygen-vacancy rich due to the aliovalent Ca^{2+} substitution at the Bi^{3+} site [35]. Oxygen vacancies are known to structurally order in these compounds as also demonstrated

by other researchers [40,41]. These oxygen vacancies are charge compensated by cosubstitution of Ca^{2+} and Ti^{4+} in BCFTO [37]. A complementary evidence for the presence of oxygen vacancies is provided by the Raman spectral analysis of characteristic two-phonon mode ($\sim 1200 \text{ cm}^{-1}$) in BiFeO_3 [42,43]. The two-phonon mode is a direct manifestation of Fe-O bond activity in the structure. Presence of V_O alters the FeO_6 octahedral arrangement resulting in a systematic variation of positions and relative intensities of two-phonon modes as detailed in the Supplemental Material [38] Sec. II and Fig. S4 [36,44]. Increased surface V_O due to the reduction of grain sizes are noted in these $\text{Bi}_{1-x}\text{Ca}_x\text{Fe}_{1-y}\text{Ti}_y\text{O}_{3-\delta}$ ceramics. Oxygen vacancies influence the electronic structure significantly, and hence we expect changes in the intrinsic magnetoelectric coupling. To infer the effect of oxygen vacancy-related structural variations on the intrinsic MD coupling, we carried out detailed MD studies.

Magnetodielectric measurements on the SPS pellets were measured at 10 and 300 K using Agilent 4284A LCR meter at a frequency of 1 MHz in a parallel plate capacitor configuration with an applied *ac* peak voltage (V_{peak}) of 1 V. The pellets were loaded in a Quantum Design physical property measurement system (PPMS), where the applied magnetic field is swept between +5 T to –5 T at a rate of $5 \times 10^{-3} \text{ T/s}$. The capacitance was recorded as a function of magnetic field using the LABVIEW program. The MD variation is estimated from the magnetocapacitance using the following equation:

$$\text{MD}\% = \left[\left(\frac{\varepsilon(H)}{\varepsilon(0)} \right) - 1 \right] \times 100\%,$$

where $\varepsilon(H)$ is the dielectric constant at an applied field H , and $\varepsilon(0)$ is the dielectric constant under $H = 0$ Oe. Magnetic hysteresis measurements (M vs H) for both AP and AA SPS pellets were done at 20 K and 300 K on a Quantum Design magnetic property measurement system MPMS superconducting quantum interference device vibrating sample magnetometer (SQUID VSM) with a maximum applied field of ± 7 T. ZFC and FC temperature-dependent magnetization measurements were done by varying the temperature from 20 to 300 K at a fixed magnetic field of 500 Oe using SQUID-VSM. Magnetoresistance measurements were done with an applied magnetic field of 0 and 5 T using a Quantum Design PPMS.

III. RESULTS AND DISCUSSION

The MD constant as a function of applied field measured on all AP and AA SPS pellets is shown in Fig. 1. Both AP and AA samples at 10 K show a negative MD effect. Pure BFO in both AP and AA conditions shows very low negative response ($\text{MD} = -0.06\%$ at $H = 5$ T). MD response increases significantly with Ca and Ca-Ti substitution. BC5FO-AP and BC5FT5O-AP pellets show a large MD change ($\sim -9.5\%$ and -10% at $H = 5$ T) compared to that of pure BFO (Table I). With increasing doping concentration, the MD response in BC10FO-AP and BC10FT100-AP samples reduced to $\sim -0.07\%$ and -1% , respectively [Fig. 1(a)]. After air-annealing, all the samples show reduced response with $\text{MD} < -0.5\%$, except BC10FT100 with $\text{MD} = -2\%$ [Fig. 1(b)]. On the other hand, at 300 K, pure BFO-AP remained to

TABLE I. Saturation magnetization (M_S) and MD response of as-prepared (AP) and air-annealed (AA) $\text{Bi}_{1-x}\text{Ca}_x\text{Fe}_{1-y}\text{Ti}_y\text{O}_{3-\delta}$ ceramics at low (10 or 20 K) and high (300 K) temperatures. BFO, BC5FO, BC10FO, BC5FT50, and BC10FT100 correspond to $x = y = 0$, $x = 0.05$; $y = 0, x = 0.1$; $y = 0, x = y = 0.05$ and $x = y = 0.1$, respectively.

Sample	Saturation magnetization M_S in emu/g (and in μ_B/Fe^{3+})				Magnetodielectric response in % at 5 T			
	20 K		300 K		10 K		300 K	
	AP	AA	AP	AA	AP	AA	AP	AA
BFO	0.63 (0.04)	0.63 (0.04)	0.62 (0.04)	0.59 (0.03)	-0.06	-0.01	-0.02	+0.08
BC5FO	2.84 (0.16)	2.81 (0.16)	2.70 (0.15)	2.77 (0.16)	-9.52	-0.16	-1.89	+0.65
BC10FO	7.82 (0.44)	5.80 (0.32)	7.32 (0.41)	5.20 (0.29)	-0.07	-0.04	+3.42	+0.07
BC5FT50	5.23 (0.29)	3.96 (0.22)	4.88 (0.27)	3.54 (0.20)	-9.96	-0.11	-1.05	+0.55
BC10FT100	10.43 (0.58)	6.40 (0.36)	9.27 (0.52)	5.77 (0.32)	-0.97	-2.01	+2.63	+2.65

show a small negative response ($\text{MD} = -0.02\%$ at $H = 5$ T), while pure BFO-AA showed a positive response. BC5FO and BC5FT50, which displayed maximum negative MD response at 10 K, showed a partial positive response at low fields ($< \pm 2$ T) and a gradual switch over to the negative values at higher fields ($H > \pm 2$ T). BC10FO and BC10FT100, which exhibited lower negative MD value at 10 K, totally switched over to an increased positive response of +3.42% and +2.63%, respectively at 300 K. The flat trend of the MD curves above $H = 2$ T seen in BC10FT100-AP suggests that a small negative component counteracts the positive value at higher fields resulting in an apparently field-independent response. After air annealing, all the samples switched to a positive MD response with a maximum of $\sim 3\%$ in BC10FT100-AA. From these measurements, we observed that the MD response is predominantly negative at low temperature and switches to a positive response at room temperature. The coexistence of negative and positive MD variation in some samples at a given temperature suggests a distinct origin for these responses.

To infer the role of magnetization on the MD effect, we measured the magnetization characteristics in these bismuth ferrite systems. Figure 2 shows the magnetic hysteresis plots

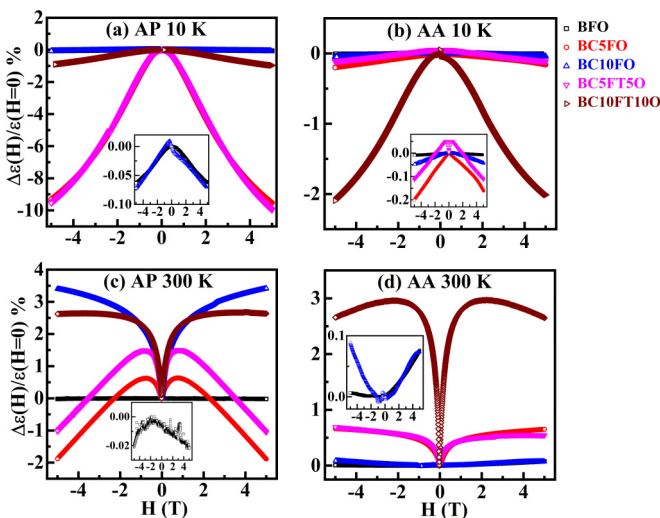


FIG. 1. Magnetodielectric response of (a), (c) as-prepared (AP) and (b), (d) air-annealed (AA) $\text{Bi}_{1-x}\text{Ca}_x\text{Fe}_{1-y}\text{Ti}_y\text{O}_{3-\delta}$ ceramics at (a), (b) 10 K and (c), (d) 300 K. The insets show the magnified plots.

(M vs H) for both AP and AA SPS pellets measured at 20 and 300 K. The magnetization values obtained from the measurements are listed in Table I. Both BFO-AP and BFO-AA show linear variation at high fields ($H > 1$ T), suggesting the samples' antiferromagnetic nature. At low fields, they exhibit weak magnetization of $M \sim 0.63$ emu/g [inset Fig. 2(a)]. BCFO and BCFTO show significantly higher magnetization due to their considerably smaller grain size compared to that of pure BFO. Surface as well as bulk V_O present in the BCFO and BCFTO are the main sources of enhanced magnetization [35,37]. However, BCFTO showed higher magnetization than BCFO in both AP and AA samples at both 20 and 300 K. Air-annealing of the pellets decreased the magnetization in magnitudes specific to the sample. A comparison of the magnetization values is given in Table I.

Figure 3 shows ZFC and FC magnetization curves ($H = 500$ Oe) of both AP and AA samples from 20 to 300 K. A striking feature observed in all the ZFC-FC curves is the sharp transition at ~ 120 K, particularly for all the AP samples.

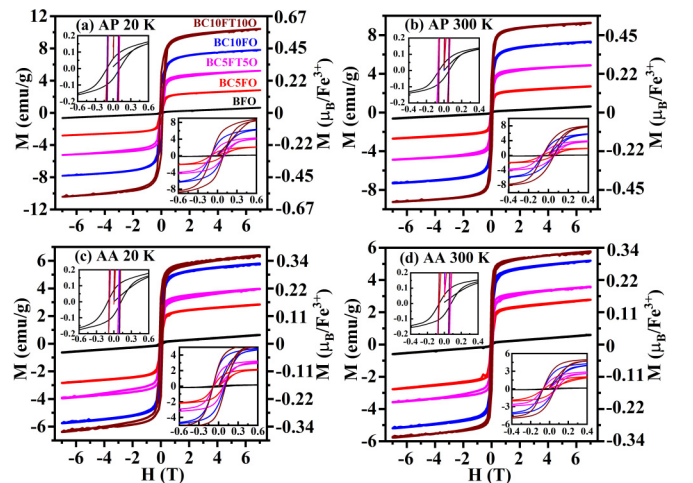


FIG. 2. Magnetization (M) vs applied magnetic field (H) curves for (a), (b) as-prepared (AP) and (c), (d) air-annealed (AA) $\text{Bi}_{1-x}\text{Ca}_x\text{Fe}_{1-y}\text{Ti}_y\text{O}_{3-\delta}$ ceramics. M - H curves are shown at two different temperatures (a), (c) 20 K and (b), (d) 300 K for AP and AA pellets. Magnified region of M - H curves near center are shown in the inset of corresponding figure. BFO, BC5FO, BC10FO, BC5FT50, and BC10FT100 correspond to $x = y = 0$, $x = 0.05$; $y = 0, x = 0.1$; $y = 0, x = y = 0.05$ and $x = y = 0.1$, respectively.

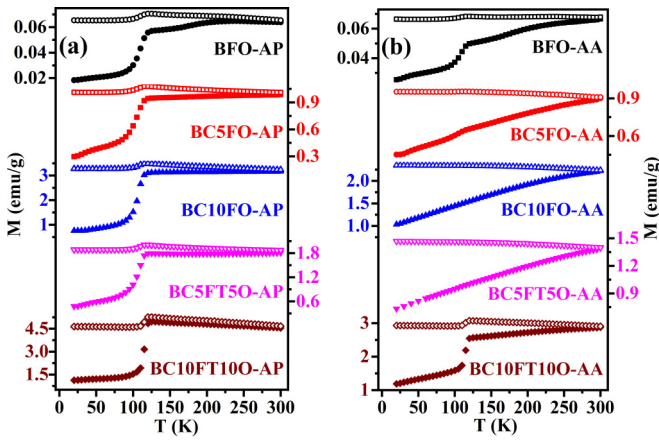


FIG. 3. Zero-field-cooled (ZFC) and field-cooled (FC) plots for (a) as-prepared (AP) and (b) air-annealed (AA) $\text{Bi}_{1-x}\text{Ca}_x\text{Fe}_{1-y}\text{Ti}_y\text{O}_{3-\delta}$ ceramics. BFO, BC5FO, BC10FO, BC5FT5O, and BC10FT10O correspond to $x = y = 0$, $x = 0.05$; $y = 0$, $x = 0.1$; $y = 0$, $x = y = 0.05$ and $x = y = 0.1$, respectively.

The change in the magnetic moment around this transition is found to be small for BFO ($\Delta m = 0.04$ emu/g), and increases with Ca substitution ($\Delta m = 0.4$ and 1.6 emu/g for $x = 0.05$ and 0.1 , respectively) and Ca-Ti cosubstitution [$\Delta m = 2$ and 4 emu/g for $x(=y) = 0.05$ and 0.1 , respectively]. Interestingly, this transition is suppressed in the AA samples with retained visibility in BFO and BC10FT10O-AA.

Bismuth ferrite is known to show several transitions in the low-temperature region. Singh *et al.* [45] have shown a spin-glass behavior below 120 K for BiFeO_3 single crystal. Surface effects studied by Jarrier *et al.* [46] showed that phase transition is accompanied with a change in lattice parameter and charge density at 140.3 K. Onset of glassy behavior was also noted at 201 K, suggesting a strong interaction between the structural strain and spin [46]. Acentric long-range spin-glass behavior in BiFeO_3 is discerned from the variation of spin-freezing temperature (T_f) with magnetic field according to the relation $T_f \propto H^{2/3}$ [47]. Unlike these observations, AC susceptibility (χ^{ac}) measurements on the SPS pellets of present study do not show any such changes with frequency (Fig. S8). This indicates that the transition observed in the ZFC-FC curves around 120 K is not the spin-glass type. Another possibility is a Verwey transition at 120 K, which is most commonly reported in Fe_3O_4 or other defective iron oxide systems [33]. This transition is accompanied by a discontinuity in the magnetic moment, resistivity, and specific heat in Fe_3O_4 [48]. Some studies suggest that the Verwey transition is related to the metal-oxygen stoichiometry in Fe_3O_4 [49,50]. This transition is also marked by the onset of charge-ordering leading to a metal-insulator (or vice versa) conversion accompanied by a structural change [48,51]. Such a Verwey transition is reported in various compounds where charge ordering is possible [52]. Therefore, the sharp transition observed in ZFC curves is correlated to the oxygen vacancy ordering that is well reported in Ca-doped BiFeO_3 [53].

Samples exhibiting a sharp transition in ZFC plots were tested for the temperature-dependent resistivity behavior at

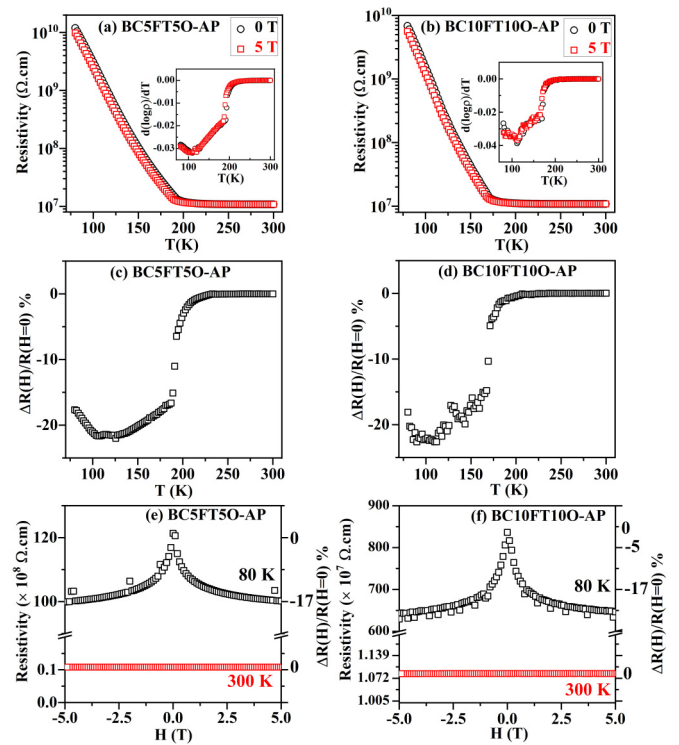


FIG. 4. (a), (b) Resistivity *vs* temperature curves for (a) BC5FT5O-AP and (b) BC10FT10O-AP ceramics with and without field. Insets show the derivative of the log of resistivity *vs* temperature plot. (c), (d) Change in magnetoresistance with the variation of temperature for (c) BC5FT5O-AP and (d) BC10FT10O-AP ceramics. (e), (f) Change in resistivity with the variation of the magnetic field at temperatures 80 and 300 K for (e) BC5FT5O-AP and (f) BC10FT10O-AP ceramics.

0 T and 5 T (Fig. 4). BFO and BCFO samples were found to be highly resistive, and temperature-dependent resistivity could be measured only for BCFTO samples. Resistivity in BCFTO does not show any obvious sign of transition at ~ 120 K (Fig. 4); however, a small change is observed from the differential resistivity plot at 120 K [inset of Figs. 4(a) and 4(b)]. The magnetoresistance $[(R(H) - R(0))/R(0)]$ plots also show this transition clearly [Figs. 4(c) and 4(d)], consistent with the Verwey-like transition observed in ZFC plots. X-ray absorption near-edge structure studies carried out on the AP and AA samples confirm the presence of Fe predominantly in $+3$ oxidation state without any indication of mixed Fe valency [37]. These studies, in combination with the temperature-dependent resistivity variation, exclude the possibility of Fe_3O_4 in our samples. Thus, the transition observed at 120 K is associated with oxygen vacancies present in the AP samples. The resistivity and magnetoresistance plots show another sharp change ~ 180 K that arises due to the temperature-dependent change in polaronic conductivity by electron and hole hopping [35,37]. It is interesting to note that the negative magnetoresistance found below 180 K switches over to zero above this temperature.

The temperature-dependent MD measurements (plotted using normalized MD with respect to the value found at 10 K) carried out with an applied magnetic field of 5 T show a

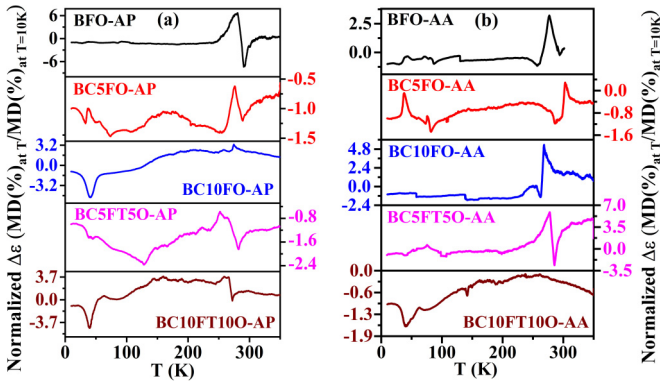


FIG. 5. Temperature-dependent normalized MD response of (a) as-prepared and (b) air annealed ceramics. Normalization is done with respect to the MD values found at 10 K temperature.

gradual change from negative to positive MD (Fig. 5), except for the abrupt large fluctuations at ~ 40 K and 250–280 K. These are reported to be spin-glass-like phase transition (~ 40 K) and antiferromagnetic transition of secondary phase $\text{Bi}_2\text{Fe}_4\text{O}_9$ (~ 264 K) in BiFeO_3 . The possible origin of such anomalous fluctuations from spurious sources like trapped O_2 (melting point, m.p. ~ 50 K) and H_2O (m.p. 273 K) molecules in ceramic pellets has been verified using Fourier transform infrared (FTIR), Raman and differential scanning calorimetry (DSC) measurements (Fig. S6 to S7 summarized in the Supplemental Material [38] Sec. III; also see references therein [54–60]). A detailed analysis of these data has confirmed the absence of any such trapped molecules in SPS pellets. Most importantly, we do not observe any abrupt changes around 120 K, suggesting that the Verwey transition in ZFC has no contribution to the total MD response.

Apart from the intrinsic magnetoelectric coupling, other factors like magnetoresistance (MR) (Maxwell-Wagner effects) can show MD response [30–32]. The possible contribution of magnetoresistive and interface effects to the overall MD response as suggested by Catalan [30] can be ruled out in the present study since all the MD measurements were carried out at 1 MHz. Further, dc MR measurements carried out on the most conductive samples (BC5FT50-AP and BC10FT100-AP) show no MR at room temperature and very negligible MR at 80 K (Fig. 4). Due to the highly resistive nature of the sample ($>10^9 \Omega \text{ cm}$), any contribution to the MD effect due to the tunneling MR will also be negligible [61]. Resistivity measurements at 10 K are limited by the sensitivity of the measurement set up used.

If the MD response originates solely from the inherent magnetoelectric coupling, then it can be expressed by Ginzburg-Landau's theory [31]. Coupling between magnetization (M) and polarization (P) is expressed by free energy

$$F = \frac{1}{2}\varepsilon_0 P^2 - PE - \alpha PM + \beta PM^2 + \gamma P^2 M^2,$$

where ε_0 is dielectric susceptibility, E is the external electric field and α , β and γ are coupling constants. Lawes *et al.* [62,63] have reported that the scalar biquadratic term $P^2 M^2$ in the free energy expansion cannot be valid in antiferromagnetic materials with limited magnetic ordering and indicated the possibilities for observing high MD response even in

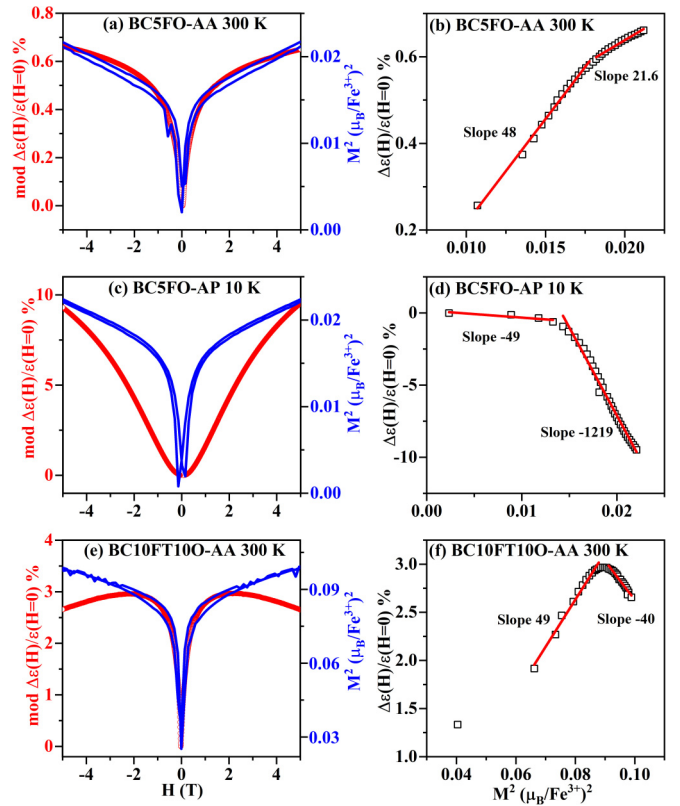


FIG. 6. (a), (c), (e) Overlap plots of squared magnetization and modulus of MD response as a function of the magnetic field and (b), (d), (f) MD response $[\Delta\varepsilon(H)/\varepsilon(H=0)]$ as a function of squared magnetization (M^2) (H) of (a), (b) BC5FO-AA at 300 K (c), (d) BC5FO-AP at 10 K and (e), (f) BC10FT100-AA at 300 K. (b), (d), (f) Open symbols show the measured data and solid lines are the linearly fitted curves.

the absence of magnetoelectric coupling. The MD effect is observed to be stronger in many antiferromagnetic materials than ferromagnets [63]. The dielectric constant is determined by the second derivative of the free energy with respect to polarization, as detailed in the following equations:

$$\frac{\partial^2 F}{\partial P^2} = \frac{1}{\chi_e} = \varepsilon_0 + 2\gamma M^2;$$

$$\varepsilon = 1 + \chi_e \approx 1 + \frac{1}{\varepsilon_0} \left(1 - 2\gamma \frac{M^2}{\varepsilon_0} \right).$$

The dielectric constant and hence the MD response is proportional to M^2 as given by the simple relation $[\varepsilon(H) - \varepsilon(0)]/\varepsilon(0) = \gamma M^2$, where $\varepsilon(H)$ and $\varepsilon(0)$ are the dielectric constants in the presence and absence of magnetic field (H), respectively, γ is MD coupling constant and M is the magnetization [64]. To check the validity of this relation in our samples, we plotted the MD response with respect to M^2 (Figs. 6 and S9–S12 in Supplemental Material [38]). Samples that exhibit only positive MD response (e.g., BC5FO-AA measured at 300 K) follow this behavior, i.e., MD *vs* H and M^2 *vs* H plots show similar trends in the entire field region [Fig. 6(a)]. The linear dependence of MD with M^2 can be inferred, as shown in Fig. 6(b). This agreement between the

M^2 and the change in dielectric constant as a function of field demonstrates a strong MD coupling.

M^2 and MD as a function of the applied field do not follow the same trend for samples exhibiting predominant negative MD response (e.g., BC5FO-AP measured at 10 K) [Fig. 6(c)], despite the observation of linear dependence with two widely different slopes in the MD *vs* M^2 plot [Fig. 6(d)]. Since these samples display a small negative MR (Fig. 4), the contribution from the interplay of MR and Maxwell-Wagner effect to the total MD response cannot be excluded. However, Maxwell-Wagner-type MR is effective only at low frequencies as the charge carriers fail to respond at relatively higher frequencies (1 MHz). In the present study, the Maxwell-Wagner-type MR contribution to the total MD response can be neglected as all the measurements reported herein were carried out at high frequencies (1 MHz) [30,64].

Interestingly, the MD response in most of the samples studied show a coexistence of positive and negative trends, the negative effect dominating at low temperature and the positive MD effect at high temperature. Figures 6(e) and 6(f) show one such example (BC10FT100-AA measured at 300 K) where the coexistence of positive and negative MD is discerned. Two linear fits—one with a positive slope at low magnetization values and the other with a negative slope from high magnetization values—can be seen from the MD *vs* M^2 plot [Fig. 6(f)]. The changes in squared magnetization (M^2) with an applied external magnetic field (H) follow a similar trend as that of MD *vs* H behavior in the low field region (<1 T), suggesting a strong inherent MD response in the presence of an applied magnetic field.

Apart from the three distinct cases discussed for their MD behavior, all the other samples show the coexistence of negative and positive MD effects with different extent of mixing (Fig. S9 to S12). These samples exhibit a linear trend for both the positive and negative MD coupling (Fig. S9 to S12). At the low magnetic field, MD *vs* H and M^2 *vs* H curves overlap [Fig. 6(e)], suggesting the domination of positive MD response due to the inherent MD coupling. The negative MD response begins to dominate at high magnetic fields (> ± 2 T) or at low temperatures. This could be activated by the spin-phonon coupling, which dominates even at high frequency under the applied field and at low temperatures. As the temperature is increased from 10 to 300 K, the negative MD effect gradually changes to a positive MD effect for all the samples (Fig. 5). The gradual changeover also suggests a linear dependence of both the negative and positive MD with temperature. The negative MD response decreases linearly with temperature, whereas the positive MD response increases.

Evidently, the MD response observed in bismuth ferrite samples depends on the sample composition, specifically the V_O . Samples with a moderate concentration of V_O viz., BC5FO-AP and BC5FT50-AP, show a large negative MD response at low temperature (10 K). Whereas the samples with higher doping concentration (and hence more V_O) show a considerable reduction in the MD response with values comparable to that observed in undoped BFO-AP at the same temperature (10 K). This clearly implies a significant role of oxygen vacancies in tuning the MD response in BiFeO₃. A definite concentration of these defects enhances both the

ferroelectric and magnetic responses in this system aiding the magnetoelectric coupling. Excess of oxygen vacancies (in case of large doping concentration; here BC10FO and BC10FT100) disturb the ferroelectric property [65] thereby reducing the magnetoelectric component. Confirming this analysis, all the air-annealed pellets showed a reduced negative MD response due to the suppression of V_O . Reduction of V_O after air-annealing has shown to decrease the magnetization and a subsequent increase in ferroelectric properties. BC10FT100-AA is an exception, as seen from the MD measurement at 10 K, due to the incomplete suppression of V_O . The observation of negative to positive MD switching response with the increase of temperature from 10 to 300 K, further asserts the dominant contribution from the inherent MD response at a higher temperature.

The large negative MD response corroborates with the structural disorder introduced by the Ca and Ca-Ti aliovalent substitutions and the smaller grain size resulting due to these dopants. The magnetization increase can be correlated either to the aliovalent substitution (like in Ca²⁺ substitution) or to the size of the particle (as in Ca-Ti co-substitution) due to the termination of spin cycloid in the BiFeO₃ structure [44]. However, to retain such a large MD effect, maintaining the ferroelectric nature upon cation doping is also necessary. Ca substitutions beyond 5 at. % seem to drastically reduce the ferroelectric polarization [65], thus suppressing the negative MD effect.

The exact origin of negative MD effect in the present study could not be understood. However, apart from the inherent magnetoelectric coupling, there can be contribution from the magnetoresistive effect, spin-phonon, and spin-lattice coupling [30,31,62]. Spin-phonon coupling plays a dominant role in MD effect at high frequencies in Mn₃O₄ [66], SeCuO₃ [63], and TeCuO₃ [63]. Further, external magnetic-field-driven electric dipoles can distort local lattice, thus resulting in a MD effect [67]. Reports on hexaferrite BaFe_{10.2}Sc_{1.8}O₁₉ suggest that both magnetoelectric type and nonmagnetoelectric spin-phonon-type coupling can generate a MD effect, with the former found to be negligible in the measured frequency range of 20 Hz to 2 MHz [64].

In the present study, observation of linear variation $\frac{\Delta\epsilon(H)}{\epsilon(H=0)}$ *vs* M^2 plot shows predominant intrinsic MD response. Although some nonlinear variation is seen in the lower values of M^2 for each sample, the linear change in relative dielectric constant with a square of magnetization confirms that the observed MD properties of Bi_{1-x}Ca_xFe_{1-y}Ti_yO_{3- δ} ceramics are due to magnetoelectric coupling. These studies prompt that high magnetization obtained by oxygen vacancy control in bismuth ferrite can be used to tailor the MD response of the specimen, which will be useful as magnetic sensors and in magnetoelectronic applications.

IV. CONCLUSION

In conclusion, a detailed analysis of the magnetic and MD properties of Ca and Ca-Ti substituted bismuth ferrite ceramics prepared by spark plasma sintering has been carried out. As-prepared Ca²⁺ substituted samples show enhanced magnetization compared to that of pure BiFeO₃ due to the oxygen vacancy-induced perturbation of the long-range spin-cycloid.

Air-annealed ceramics show a decrease in magnetization due to the suppression of V_O . A sharp change in ZFC-FC magnetization *vs* temperature curves ~ 120 K is attributed to the Verwey-like transition mostly arising from V_O ordering in the BiFeO_3 structure. This transition diminishes in air-annealed ceramics and has no influence on the MD response. The MD response shows a gradual switch over from negative to positive values with increasing temperature from 10 to 300 K. A maximum negative MD response, $\frac{\Delta\varepsilon(H)}{\varepsilon(H=0)}$, of $\sim -10\%$ is observed in AP 5 at. % Ca and Ca-Ti substituted BiFeO_3 ceramics at 10 K. At 300 K, all these same samples show either positive or coexistence of positive and negative MD response. A maximum positive response with $\frac{\Delta\varepsilon(H)}{\varepsilon(H=0)} = +3.4\%$ at 5 T is observed for 10 at. % Ca and Ca-Ti substituted BiFeO_3 ceramics. In all the samples, a linear dependence of MD *vs* M^2 is noted. However, positive MD effect followed the same trend for the M^2 *vs* H and $\frac{\Delta\varepsilon(H)}{\varepsilon(H=0)}$ *vs* H suggesting strong inherent MD coupling. On the other hand, the negative MD effect does not follow this trend. Contribution from other factors like spin-phonon coupling, spin-lattice coupling, and lattice distortion can promote the negative MD effect. MD measurement made at 1 MHz and the absence of magnetoresistance at 300 K exclude the Maxwell-Wagner effect contributions to

the MD response. Similarly, neither the Verwey-like transition (~ 120 K) nor the temperature-dependent change in the polaronic conductivity (~ 180 K) has any influence on the MD response. On the other hand, large fluctuations in MD observed at ~ 40 K and ~ 250 – 280 K are attributed to the spin-glass-like phase transition and antiferromagnetic transition of $\text{Bi}_2\text{Fe}_4\text{O}_9$, respectively. While V_O promotes large magnetization, it diminishes ferroelectric ordering. Therefore, optimum V_O is required to achieve a large MD response. This study explicitly highlights the influence of oxygen vacancies on the MD response in BiFeO_3 . The large MD response observed in these bismuth ferrite ceramics can be used for magnetoelectric sensor applications.

ACKNOWLEDGMENTS

C.S. acknowledges the support from Department of Science and Technology, Science and Engineering Research Board (DST-SERB) through Grant No. EMR/2016/002785. C.S. also acknowledges the support by MHRD, India through the Institutes of Eminence (vide SP20210777DRMHRDDIRIIT) for the research initiatives on establishing the prospective Centre for Advanced Materials and Microscopy (vide SB20210844MMMHRD008277).

-
- [1] M. Fiebig, *J. Phys. D* **38**, R123 (2005).
 [2] N. A. Hill, *J. Phys. Chem. B* **104**, 6694 (2000).
 [3] H. Béa, M. Gajek, M. Bibes, and A. Barthélémy, *J. Phys. Condens. Matter* **20**, 434221 (2008).
 [4] M. Bibes and A. Barthélémy, *Nat. Mater.* **7**, 425 (2008).
 [5] S. Murakami, N. T. A. F. Ahmed, D. Wang, A. Feteira, D. C. Sinclair, and I. M. Reaney, *J. Eur. Ceram. Soc.* **38**, 4220 (2018).
 [6] M. Dziubaniuk, R. Bujakiewicz-Korońska, J. Suchanicz, J. Wyrwa, and M. Rękas, *Sens. Actuators B* **188**, 957 (2013).
 [7] S. D. Waghmare, V. V. Jadhav, S. F. Shaikh, R. S. Mane, J. H. Rhee, and C. O'Dwyer, *Sens. Actuators A* **271**, 37 (2018).
 [8] J. Wang, J. B. Neaton, H. Zheng, V. Nagarajan, S. B. Ogale, B. Liu, D. Viehland, V. Vaithyanathan, D. G. Schlom, U. V. Waghmare, N. A. Spaldin, K. M. Rabe, M. Wuttig, and R. Ramesh, *Science* **299**, 1719 (2003).
 [9] C. Ederer and N. A. Spaldin, *Phys. Rev. B* **71**, 060401(R) (2005).
 [10] A. H. Khan, S. Atiq, M. S. Anwar, S. Naseem, and S. K. Abbas, *J. Mater. Sci. Mater. Electron.* **29**, 11812 (2018).
 [11] Y. Bai, S. W. Wang, X. Zhang, Z. K. Zhao, Y. P. Shao, R. Yao, M. M. Yang, and Y. B. Gao, *Mater. Res. Express* **6**, 026101 (2018).
 [12] M. G. Masud, B. K. Chaudhuri, and H. D. Yang, *J. Phys. D* **44**, 255403 (2011).
 [13] S. Tiwari and S. Vitta, *Sci. Rep.* **8**, 11619 (2018).
 [14] P. Pan, J. Tao, F. Ma, and N. Zhang, *J. Magn. Magn. Mater.* **453**, 91 (2018).
 [15] D. K. Pradhan, V. S. Puli, S. N. Tripathy, D. K. Pradhan, J. F. Scott, and R. S. Katiyar, *J. Appl. Phys.* **114**, 234106 (2013).
 [16] S. He, G. Liu, J. Xu, J. Yang, Y. Chen, S. Kang, S. Yan, and L. Mei, *Mater. Lett.* **89**, 159 (2012).
 [17] V. V. Lazenka, G. Zhang, J. Vanacken, I. I. Makoed, A. F. Ravinski, and V. V. Moshchalkov, *J. Phys. D* **45**, 125002 (2012).
 [18] A. Kumar and K. L. Yadav, *J. Alloys Compd.* **554**, 138 (2013).
 [19] A. Rathi, A. Anshul, A. Gupta, P. K. Rout, K. K. Maurya, R. K. Kotnala, R. P. Pant, and G. A. Basheed, *J. Phys. D* **50**, 135006 (2017).
 [20] K. F. Wang, J. M. Liu, and Z. F. Ren, *Adv. Phys.* **58**, 321 (2009).
 [21] A. Mukherjee, S. Basu, P. K. Manna, S. M. Yusuf, and M. Pal, *J. Mater. Chem. C* **2**, 5885 (2014).
 [22] J. Kolte, A. S. Daryapurkar, M. Agarwal, D. D. Gulwade, and P. Gopalan, *Mater. Chem. Phys.* **193**, 253 (2017).
 [23] D. P. Dutta, B. P. Mandal, R. Naik, G. Lawes, and A. K. Tyagi, *J. Phys. Chem. C* **117**, 2382 (2013).
 [24] A. Kumar, K. L. Yadav, S. Kumar, N. Kumar, A. Mishra, N. Kumar, U. Shankar, T. Mehrotra, G. Sharma, R. Kumar, and G. D. Adhikary, *J. Phys. Chem. Solids* **124**, 19 (2019).
 [25] D. P. Dutta and A. K. Tyagi, *Appl. Surf. Sci.* **450**, 429 (2018).
 [26] Y. F. Cui, Y. G. Zhao, L. B. Luo, J. J. Yang, H. Chang, M. H. Zhu, D. Xie, and T. L. Ren, *Appl. Phys. Lett.* **97**, 222904 (2010).
 [27] P. Singh and J. H. Jung, *Physica B* **405**, 1086 (2010).
 [28] A. Kumar and K. L. Yadav, *Physica B* **405**, 4650 (2010).
 [29] A. Mukherjee, S. Basu, L. A. W. Green, N. T. K. Thanh, and M. Pal, *J. Mater. Sci.* **50**, 1891 (2015).
 [30] G. Catalan, *Appl. Phys. Lett.* **88**, 102902 (2006).
 [31] T. Kimura, S. Kawamoto, I. Yamada, M. Azuma, M. Takano, and Y. Tokura, *Phys. Rev. B* **67**, 180401(R) (2003).
 [32] S. Chatterjee, R. Maiti, and D. Chakravorty, *RSC Adv.* **10**, 13708 (2020).

- [33] S. K. Park, T. Ishikawa, and Y. Tokura, *Phys. Rev. B* **58**, 3717 (1998).
- [34] S. Nandy, P. S. V. Mocherla, and C. Sudakar, *J. Appl. Phys.* **121**, 203102 (2017).
- [35] S. Nandy, K. Kaur, P. S. V. Mocherla, B. R. K. Nanda, and C. Sudakar, *J. Appl. Phys.* **124**, 195108 (2018).
- [36] P. S. V. Mocherla, M. B. Sahana, R. Gopalan, M. S. Ramachandra Rao, B. R. K. Nanda, and C. Sudakar, *Mater. Res. Express* **4**, 106106 (2017).
- [37] S. Nandy, P. S. V. Mocherla, K. Kaur, S. Gautam, B. R. K. Nanda, and C. Sudakar, *J. Appl. Phys.* **126**, 235101 (2019).
- [38] See Supplemental Material at <http://link.aps.org/supplemental/10.1103/PhysRevB.103.184406> for x-ray diffraction, FESEM images and a summary of results on oxygen vacancy in $\text{Bi}_{1-x}\text{Ca}_x\text{Fe}_{1-y}\text{Ti}_y\text{O}_{3-\delta}$ ceramics. FTIR, Raman, and DSC studies on $\text{Bi}_{1-x}\text{Ca}_x\text{Fe}_{1-y}\text{Ti}_y\text{O}_{3-\delta}$ ceramics are included. AC susceptibility vs temperature curves of BC10FO-AP ceramics is shown. Magnetodielectric response as a function of squared magnetization and the overlap plots of squared magnetization and MD response as a function magnetic field of these ceramics are shown.
- [39] P. S. V. Mocherla, S. Gautam, K. H. Chae, M. S. R. Rao, and C. Sudakar, *Mater. Res. Express* **2**, 095012 (2015).
- [40] R. L. Withers, L. Bourgeois, K. Balamurugan, N. Harish Kumar, P. N. Santhosh, and P. M. Woodward, *J. Solid State Chem.* **182**, 2176 (2009).
- [41] R. L. Withers, J. Schiemer, L. Bourgeois, L. Norén, and Y. Liu, *J. Phys. Conf. Ser.* **226**, 012015 (2010).
- [42] M. Cazayous, A. Sacuto, D. Lebeugle, and D. Colson, *Eur. Phys. J. B* **67**, 209 (2009).
- [43] M. O. Ramirez, M. Krishnamurthi, S. Denev, A. Kumar, S.-Y. Yang, Y.-H. Chu, E. Saiz, J. Seidel, A. P. Pyatakov, A. Bush, D. Viehland, J. Orenstein, R. Ramesh, and V. Gopalan, *Appl. Phys. Lett.* **92**, 022511 (2008).
- [44] P. S. V. Mocherla, C. Karthik, R. Ubic, M. S. R. Rao, and C. Sudakar, *Appl. Phys. Lett.* **105**, 132409 (2014).
- [45] M. K. Singh, W. Prellier, M. P. Singh, R. S. Katiyar, and J. F. Scott, *Phys. Rev. B* **77**, 144403 (2008).
- [46] R. Jarrier, X. Marti, J. Herrero-Albillos, P. Ferrer, R. Haumont, P. Gemeiner, G. Geneste, P. Berthet, T. Schüllli, P. Cevc, R. Blinc, S. S. Wong, T.-J. Park, M. Alexe, M. A. Carpenter, J. F. Scott, G. Catalan, and B. Dkhil, *Phys. Rev. B* **85**, 184104 (2012).
- [47] M. K. Singh, R. S. Katiyar, W. Prellier, and J. F. Scott, *J. Phys. Condens. Matter* **21**, 042202 (2008).
- [48] F. Walz, *J. Phys. Condens. Matter* **14**, R285 (2002).
- [49] F. J. Berry, S. Skinner, and M. F. Thomas, *J. Phys. Condens. Matter* **10**, 215 (1998).
- [50] J. P. Shepherd, R. Aragón, J. W. Koenitzer, and J. M. Honig, *Phys. Rev. B* **32**, 1818 (1985).
- [51] J. B. Yang, X. D. Zhou, W. B. Yelon, W. J. James, Q. Cai, K. V. Gopalakrishnan, S. K. Malik, X. C. Sun, and D. E. Nikles, *J. Appl. Phys.* **95**, 7540 (2004).
- [52] D. J. Huang, H. J. Lin, J. Okamoto, K. S. Chao, H. T. Jeng, G. Y. Guo, C. H. Hsu, C. M. Huang, D. C. Ling, W. B. Wu, C. S. Yang, and C. T. Chen, *Phys. Rev. Lett.* **96**, 096401 (2006).
- [53] J. A. Schiemer, R. L. Withers, Y. Liu, and M. A. Carpenter, *Chem. Mater.* **25**, 4436 (2013).
- [54] K. Nakamoto, in *Handbook of Vibrational Spectroscopy* (Wiley, New York, 2006), pp. 1872–1892.
- [55] P. Hermet, M. Goffinet, J. Kreisel, and P. Ghosez, *Phys. Rev. B* **75**, 220102(R) (2007).
- [56] S. Bashchenko and L. S. Marchenko, *Semicond. Phys. Quantum Electron. Optoelectron.* **14**, 77 (2011).
- [57] Z. Chen, Y. Li, Y. Wu, and J. Hu, *J. Mater. Sci. Mater. Electron.* **23**, 1402 (2012).
- [58] M. Amin, H. M. Rafique, M. Yousaf, S. M. Ramay, M. Saleem, S. K. Abbas, and S. Atiq, *J. Mater. Sci. Mater. Electron.* **28**, 17234 (2017).
- [59] C. Himcinschi, J. Rix, C. Röder, M. Rudolph, M.-M. Yang, D. Rafaja, J. Kortus, and M. Alexe, *Sci. Rep.* **9**, 379 (2019).
- [60] M. Vrankić, A. Šarić, S. Bosnar, D. Pajić, J. Dragović, A. Altomare, A. Falcicchio, J. Popović, M. Jurić, M. Petravić, I. J. Badovinac, and G. Dražić, *Sci. Rep.* **9**, 15158 (2019).
- [61] Y. S. Koo, T. Bonaedy, K. D. Sung, J. H. Jung, J. B. Yoon, Y. H. Jo, M. H. Jung, H. J. Lee, T. Y. Koo, and Y. H. Jeong, *Appl. Phys. Lett.* **91**, 212903 (2007).
- [62] G. Lawes, T. Kimura, C. M. Varma, M. A. Subramanian, N. Rogado, R. J. Cava, and A. P. Ramirez, *Prog. Solid State Chem.* **37**, 40 (2009).
- [63] G. Lawes, A. P. Ramirez, C. M. Varma, and M. A. Subramanian, *Phys. Rev. Lett.* **91**, 257208 (2003).
- [64] R. Tang, H. Zhou, W. You, and H. Yang, *Appl. Phys. Lett.* **109**, 082903 (2016).
- [65] S. Nandy, K. Kaur, S. Gautam, K. H. Chae, B. R. K. Nanda, and C. Sudakar, *ACS Appl. Mater. Interfaces* **12**, 14105 (2020).
- [66] R. Tackett, G. Lawes, B. C. Melot, M. Grossman, E. S. Toberer, and R. Seshadri, *Phys. Rev. B* **76**, 024409 (2007).
- [67] H. Izadkhan, S. Zare, S. Somu, and C. Vittoria, *Appl. Phys. Lett.* **106**, 142905 (2015).